www.ijarp.com ISSN 2456-9992 Page: 01-14

International Journal Advanced Research Publications

Research Article

Volume: 02

Issue: 09

OPTIMAL LOAD FREQUENCY CONTROL OF AN INTERCONNECTED POWER SYSTEM USING PSO ALGORITHM

Sonali Vijay Randive*[1], Dr. B Sampath Kumar[2], Prof. R. T. Bansode[3]

[1]M. Tech Student, Department of Electrical Engineering Dr. Babasaheb Ambedkar Technological University, Fabtech College of Engineering and Research, Sangola.

[2]Assistant Prof, Department of Electrical Engineering Dr. Babasaheb Ambedkar Technological University, Fabtech College of Engineering and Research, Sangola.

[3]Assistant Prof. Department of Electrical Engineering Dr. Babasaheb Ambedkar Technological University, Fabtech College of Engineering and Research, Sangola.

Article Received: 19 July 2026, Article Revised: 14 August 2026, Published on: 03 September 2026

***Corresponding Author: Sonali Vijay Randive**

M. Tech Student, Department of Electrical Engineering Dr. Babasaheb Ambedkar Technological University, Fabtech College of Engineering and Research, Sangola.

Doi: https://doi-doi.org/101555/ijarp.2879

ABSTRACT

Interconnected power systems require robust coupled control to maintain system frequency and tie-line power flow under sequential load disturbances. This study presents a Particle Swarm Optimization (PSO)-tuned filtered Proportional–Integral–Derivative (PSO-PID) control scheme applied to a heterogeneous three-area Load Frequency Control (LFC) system. Each area integrates an independent governor, turbine, generator–load dynamics, a frequency-bias loop, and a dedicated filtered PID controller, connected through three bilateral tie-line channels. A 30-particle swarm optimized over 50 iterations tunes nine controller gains within bounded parameters, minimizing a composite dynamic objective function. System performance was evaluated in MATLAB/Simulink under sequential step load perturbations of 0.010\text{ p.u.} at t = 1\text{ s}, 0.008\text{ p.u.} at t = 35\text{ s}, and 0.006\text{ p.u.} at t = 70\text{ s}.

KEYWORDS: Automatic Generation Control; Area Control Error; Filtered Pid Controller; Interconnected Power System; Load Frequency Control; Matlab/Simulink; Particle Swarm Optimization; Tie-Line Power.

1. INTRODUCTION

Interconnected power networks must continuously balance mechanical generation and electrical demand because even a small active-power mismatch changes rotor kinetic energy and system frequency. Load Frequency Control (LFC), implemented within Automatic Generation Control (AGC), restores nominal frequency and scheduled tie-line interchange after disturbances. The problem is increasingly demanding in heterogeneous and renewable-rich networks, where uncertain injections, unequal area dynamics and constrained actuators produce coupled oscillations. Recent reviews identify optimization-assisted secondary control as a practical route for coordinating multiple areas without relying on a single nominal operating point [1]. Comparative studies further show that conventional fixed-gain regulators may exhibit prolonged settling and sensitivity to parameter variations, motivating robust optimization of controller gains [2].

Integral, PI and PID controllers remain attractive because their implementation is transparent and compatible with existing AGC structures. Nevertheless, manual or rule-based tuning treats the areas and response measures only indirectly. Gains that suppress local frequency error can intensify tie-line oscillation or control effort, and one common gain set is unsuitable when governor, turbine and power-system time constants differ. Improved sine–cosine tuning of two-degree-of-freedom PID controllers has confirmed the value of objective-function-based design in nonlinear three-area systems [3], while JAYA- and differential-evolution-based AGC investigations demonstrate that multi-parameter searches can improve damping under distinct load scenarios [4], [5].

Particle Swarm Optimization (PSO) is well suited to LFC because it uses derivative-free population search, bounded positions and a compact velocity-update law. Each particle represents a complete controller-gain vector; simulation provides the fitness, and personal-best and global-best memories guide the swarm. PSO can therefore tune coupled controller parameters even when the cost includes non-smooth peak penalties and time-integral errors. The present work focuses on a reproducible standard PSO rather than a hybrid optimizer, establishes explicit gain bounds and uses independent filtered PID controllers for three unequal areas.

The contribution is a transparent three-area PSO–PID framework that combines area-frequency deviations, three tie-line exchanges and area-control errors within one evaluation process. The study reports exact controller gains, convergence settings, peak deviations, settling time, controller energy and integral indices. It also distinguishes aggregate improvement from channel-specific behaviour: although the overall tie-line peak decreases, the P23 channel shows a small adverse change. This distinction prevents an unsupported claim of uniform improvement and provides a technically defensible benchmark for later nonlinear, renewable-integrated and hardware-in-the-loop studies.

2. Related Work

Optimization-based LFC research has progressed from conventional PI/PID tuning toward fractional-order, fuzzy, hybrid and resilient control. A PSO–PID study of a multi-source standalone system reported faster restoration but did not explicitly model scheduled multi-area interchange [6]. PSO-based renewable LFC confirmed improved frequency damping under variable generation, although its plant architecture differs from a heterogeneous conventional three-area system [7]. Fractional-order and chaotic-PSO approaches enlarged controller flexibility, but also increased the number of tuned parameters and interpretation burden [8]. An improved swarm-based fractional controller likewise enhanced dynamic behaviour, yet its higher-order structure complicates reproducible implementation [9]. These studies support swarm tuning while leaving a need for a concise, independently tuned three-area benchmark.

Hybrid optimization has recently been adopted to improve exploration and exploitation. A PSO–Artificial Hummingbird Algorithm tuned PID controller achieved strong transient reductions in interconnected cases but required additional algorithmic mechanisms [10]. An adaptive PSO tuned cascaded FOPI–FOPIDN design addressed renewable-integrated interconnected systems; its controller order, adaptive coefficients and parameter count exceed those of a standard filtered PID benchmark [11]. Multi-area renewable studies also emphasize robustness to generation uncertainty [12]. Intelligent-controller comparisons published in 2025 continue to use PSO–PID as an interpretable reference for multi-area frequency stabilization [13], while recent hybrid and fractional designs report improved damping at the cost of more design variables [14], [15].

Robust and nonlinear LFC studies increasingly consider uncertainty, attacks and communication constraints. Fixed-time and robust nonlinear designs strengthen theoretical guarantees but depend on more detailed plant assumptions [16], [17]. Recent adaptive control studies address changing system dynamics, yet online adaptation raises validation and implementation requirements [18]. Renewable-rich multi-area analyses published in 2026 extend the operating envelope and demonstrate the need for consistent comparative benchmarks [19]. A 2026 PSO-tuned hybrid fuzzy assessment illustrates the field's movement toward rule-based intelligent control, but membership functions and rule-base selection reduce transparency [20]. Across these contributions, four recurring limitations remain: inconsistent objective functions, incomplete reporting of controller bounds, insufficient channel-wise tie-line analysis, and limited numerical-versus-simulation reproducibility. The proposed filtered PSO–PID design addresses these gaps through explicit settings, separate area gains, three tie-line channels and consolidated performance metrics.

3. Research Method

A simulation-based quantitative method is adopted. First, the three control areas are parameterized independently and connected through P12, P23 and P13 tie-line dynamics. Second, each area control error (ACE) is formed from its frequency-bias term and signed net tie-line export. Third, nine filtered-PID gains are encoded in a PSO particle. Fourth, the dynamic response to three sequential load steps is simulated and evaluated using time-integral error, peak and control-effort terms. Finally, the stable baseline and optimized controller are compared using identical plant parameters and disturbance timing.

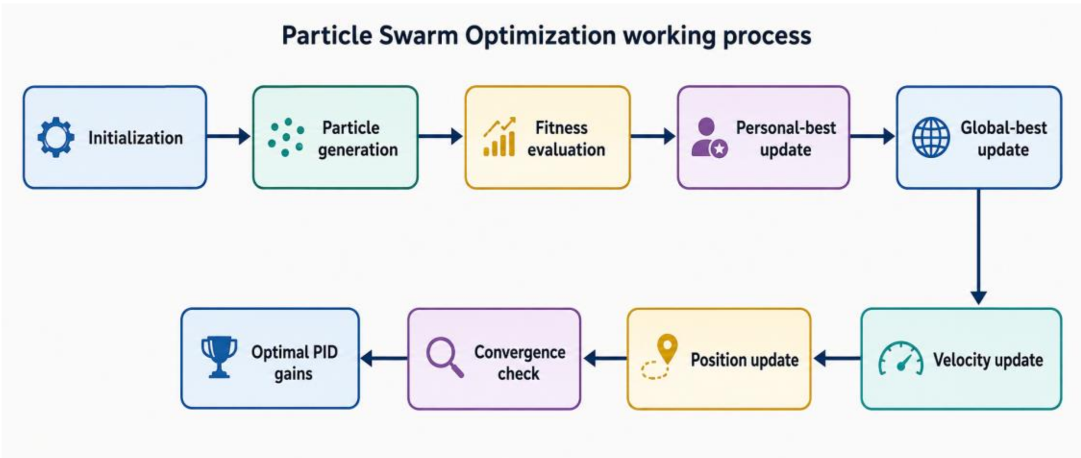

Fig. 1. PSO-Based Research and Controller-Tuning Workflow.

3.1 Particle Swarm Optimization

$$v_i^{k+1} = \omega v_i^k + c^1 r^1 (pbest_i - x_i^k) + c^2 r^2 (gbest - x_i^k) \tag{1}$$

$$x_i^{k+1} = x_i^k + v_i^{k+1} \tag{2}$$

Here, x_i and v_i denote the position and velocity of particle i; $pbest_i$ and gbest denote the best personal and global solutions; ω is the inertia weight; c_1 and c_2 are cognitive and social coefficients; and r_1 and r_2 are independent random numbers in [0,1]. The swarm contains 30 particles and runs for 50 iterations. The inertia weight decreases from 0.90 to 0.35,

$c_1=c_2=1.70$, velocity is clamped to 20% of each decision range, and random seed 7 supports repeatability. Search bounds are $0.05\leq Kp\leq 1.50$, $0.01\leq Ki\leq 0.40$ and $0\leq Kd\leq 0.10$ for every area.

3.2 Objective and Evaluation Procedure

$$IAE = \int_0^T |e(t)|dt,\ ISE = \int_0^T e^2(t)\,dt,\ ITAE = \int_0^T t|e(t)|dt \quad (3)$$

$$Improvement\ (\%) = \left[\frac{Xbaseline - XPSO}{Xbaseline}\right] \times 100 \quad (4)$$

The multi-signal error vector includes Δf_1, Δf_2, Δf_3, ΔP_{12}, ΔP_{23}, ΔP_{13} and the corresponding ACE signals. Lower integral indices, deviations and settling times indicate improvement. Controller effort is evaluated separately because aggressive regulation can reduce error while increasing actuator demand. The same 120 s simulation horizon and load sequence are retained for the baseline and optimized cases. The first, second and third load steps are 0.010, 0.008 and 0.006 p.u. at 1, 35 and 70 s, respectively.

Table 2. PSO settings and optimized filtered-PID gains.

Item	Area 1	Area 2	Area 3	Unit / setting
Kp	1.23777677	0.11868653	0.05000000	—
Ki	0.40000000	0.40000000	0.399999996	s^{-1}
Kd	0.10000000	0.09999996	0.10000000	s
Derivative filter Tf	0.08	0.08	0.08	s
Swarm size	30	30	30	particles
Iterations	50	50	50	iterations

4. Modelling and Design

Mathematical modelling establishes the dynamic relationship among generation, load demand, system frequency, and tie-line power exchange in the interconnected power system. Each control area is represented using the transfer functions of the speed governor, turbine, generator–load unit, tie-line network, and load-frequency controller. The Area Control Error combines local frequency deviation with incremental tie-line power deviation to generate the controller input. Particle Swarm Optimization is employed to determine the controller gains within the specified search bounds by minimizing the selected performance index. The resulting mathematical framework is subsequently implemented in MATLAB/Simulink to evaluate system stability and dynamic response under load disturbances.

4.1 Governor Model

$$Gg,i(s) = \Delta Pg,\frac{i(s)}{\Delta Pc},i(s) = \frac{1}{Tg,i\,s+1} \quad (5)$$

Tg,i is the governor time constant, ΔPc,i is the secondary control command corrected for droop feedback, and ΔPg,i is the governor output. Area-dependent Tg values preserve the unequal response speeds in the supplied system.

4.2 Turbine Model

$$Gt,i(s) = \Delta Pt,\frac{i(s)}{\Delta Pg},i(s) = \frac{1}{Tt,i\,s+1} \tag{6}$$

Tt,i denotes turbine time constant and ΔPt,i denotes incremental turbine mechanical power. The principal three-area system uses first-order non-reheat equivalents. The hydro–thermal configuration instead contains detailed reheat thermal and hydro turbine transfer functions, which are reported separately in Table 2.

4.3 Generator–Load Model

$$Gps,i(s) = \frac{\Delta fi(s)}{[\Delta Pt,i(s) - \Delta PL,i(s) - \Delta Ptie,i(s)]} = Kps,\frac{i}{Tps,i\,s+1} \tag{7}$$

Kps,i and Tps,i represent the equivalent area power-system gain and time constant. The equation maps incremental power imbalance into frequency deviation in per unit.

4.4 Tie-Line Model

$$\Delta Pij(s) = \left(\frac{2\pi Tij}{s}\right)[\Delta fi(s) - \Delta fj(s)] \tag{8}$$

Tij is the synchronizing coefficient. Correct signed exports are ΔPtie,1=ΔP12+ΔP13, ΔPtie,2=−ΔP12+ΔP23, and ΔPtie,3=−ΔP13−ΔP23.

4.5 Area Control Error

$$ACEi(t) = Bi\Delta fi(t) + \Delta Ptie,i(t) \tag{9}$$

Bi is the frequency-bias coefficient. Driving ACE to zero simultaneously restores local frequency and scheduled interchange.

4.6 Filtered-PID Controller

$$Ci(s) = Kp,i + Ki,\frac{i}{s} + Kd,i\frac{s}{1+Tf,i\,s} \tag{8}$$

The actual primary quantitative system uses independent filtered PID action. Tf=0.08 s in all three areas. The filter avoids an ideal derivative impulse while retaining damping. The three-area integral-control system uses integral control only, and the hydro–thermal system applies a common three-parameter PID vector to both areas; these architectures are not misreported as independent filtered PID controllers.

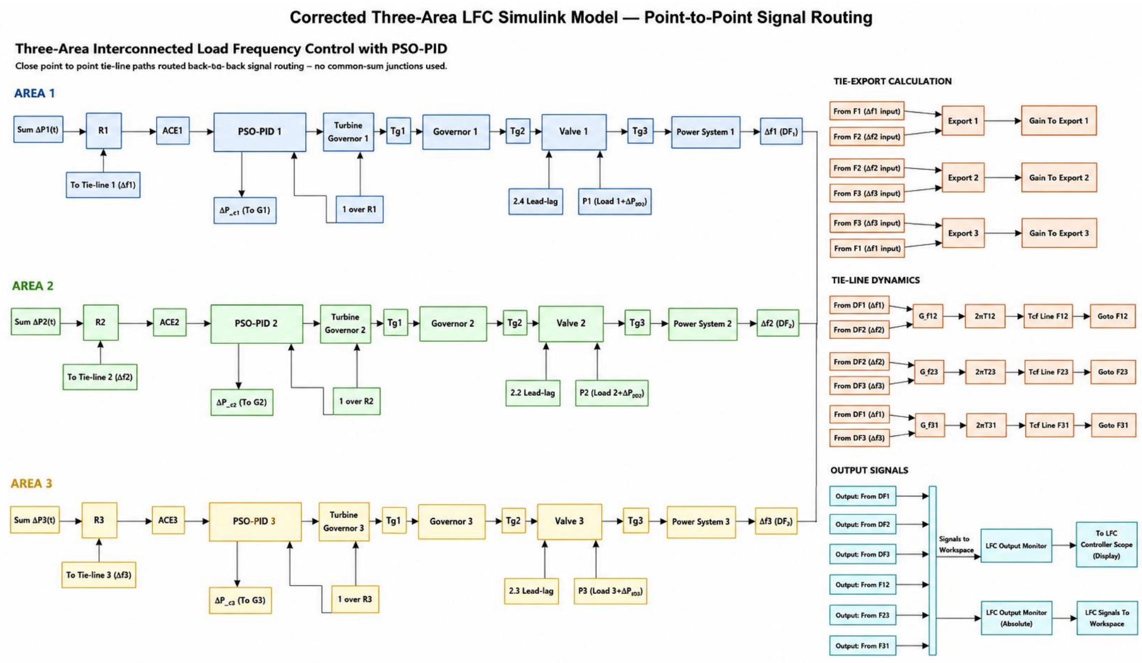

Fig. 2. Corrected heterogeneous three-area LFC architecture with independent filtered PID controllers and point-to-point signal routing.

The figure illustrates the corrected three-area interconnected Load Frequency Control system employing independently tuned PSO–PID controllers and point-to-point signal routing. In each area, the Area Control Error is processed by the corresponding PSO–PID controller before passing through turbine–governor, valve and power-system dynamics. Local load disturbances are applied separately, while frequency deviations are fed back through droop and frequency-bias paths to maintain generation–demand balance. The tie-export calculation section determines the net scheduled power exchange among Areas 1, 2 and 3. Tie-line dynamics are developed from the frequency differences between interconnected areas and their synchronizing coefficients. Finally, frequency and tie-line signals are combined through an output multiplexer for scope visualization and workspace analysis, enabling systematic evaluation of frequency regulation, inter-area coordination and controller performance.

Table 3. Heterogeneous Three-Area Power-System Parameters.

Parameter	**Area 1**	**Area 2**	**Area 3**	**Unit**
Governor time constant, Tg	0.08	0.10	0.12	s
Turbine time constant, Tt	0.30	0.33	0.35	s
Power-system time constant, Tps	20	22	24	s
Power-system gain, Kps	120	115	125	—
Speed regulation, R	2.4	2.7	2.5	—
Frequency bias, B	0.425	0.390	0.410	—
Load step / application time	0.010 / 1	0.008 / 35	0.006 / 70	p.u. / s

The figure illustrates the corrected three-area interconnected Load Frequency Control system employing independently tuned PSO–PID controllers and point-to-point signal routing. In each area, the Area Control Error is processed by the corresponding PSO–PID controller before passing through turbine–governor, valve and power-system dynamics. Local load disturbances are applied separately, while frequency deviations are fed back through droop and frequency-bias paths to maintain generation–demand balance. The tie-export calculation section determines the net scheduled power exchange among Areas 1, 2 and 3. Tie-line dynamics are developed from the frequency differences between interconnected areas and their synchronizing coefficients. Finally, frequency and tie-line signals are combined through an output multiplexer for scope visualization and workspace analysis, enabling systematic evaluation of frequency regulation, inter-area coordination and controller performance.

5. RESULTS AND DISCUSSION

The response is evaluated under three sequential area disturbances over 120 s. The stable baseline serves as the reference, and all percentage changes use the same definition in (4). The analysis separates peak response, integral error, terminal restoration and controller energy. This separation is important because a smaller tracking error does not automatically imply lower actuator effort or uniform improvement in every tie-line channel.

5.1 PSO Convergence and Frequency Response

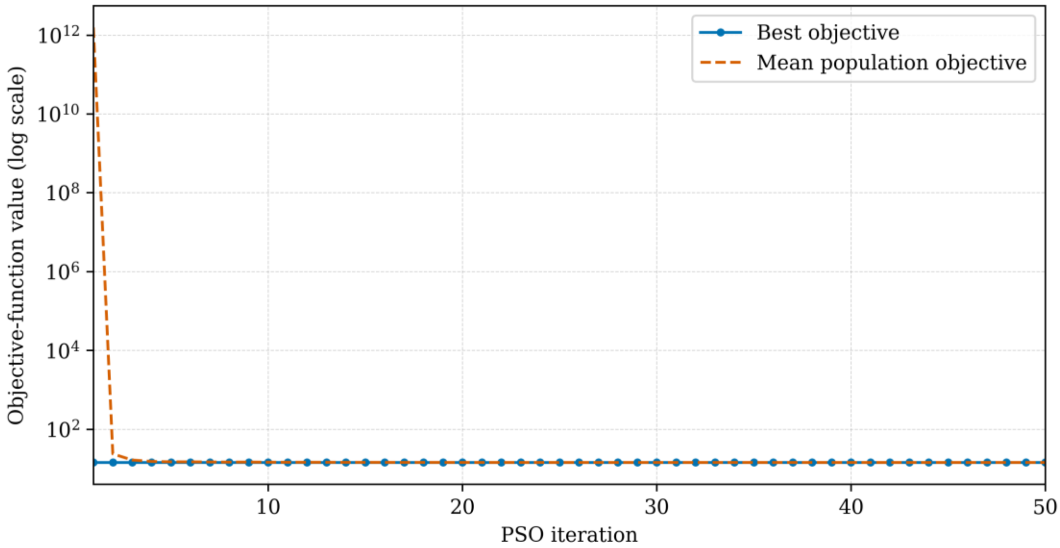

Fig. 3. Best-Cost and Mean-Cost Convergence Over 50 PSO Iterations.

Figure 3 indicates rapid contraction of the population mean during the early iterations, followed by stabilization near the best solution. The best-cost trace remains bounded and the mean approaches it, demonstrating that the reported gains are not the result of an unconstrained excursion. Because convergence is evaluated with the complete multi-area response, the optimized gains reflect coupled frequency, tie-line and ACE behaviour rather than a single local waveform.

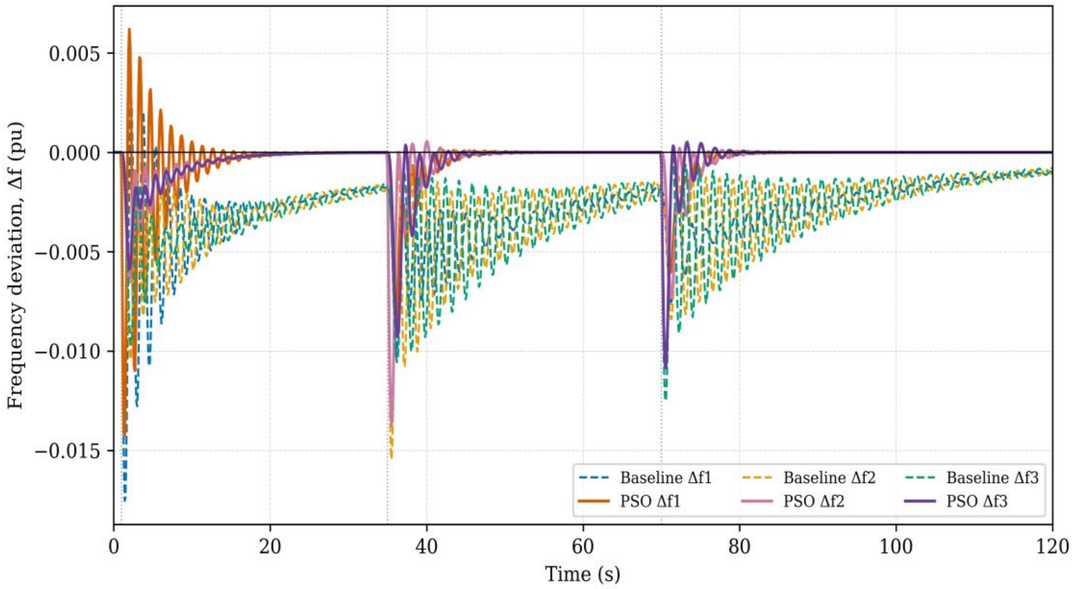

Fig. 4. Combined three-area frequency deviations for stable baseline and PSO-optimized filtered PID control.

Figure 4 shows that each load step excites all three areas, confirming the multiple-input, multiple-output character of the plant. The optimized responses decay to zero after each disturbance, whereas the baseline traces retain slow oscillatory components through the 120 s horizon. The largest absolute frequency deviation decreases from 0.017536 to 0.014238 p.u. Area-wise reductions are 18.81%, 11.02% and 13.30% for Areas 1–3, respectively. The nonuniform improvement is consistent with heterogeneous area parameters and independent gain selection.

5.2 Tie-Line, ACE and Integral-Error Performance

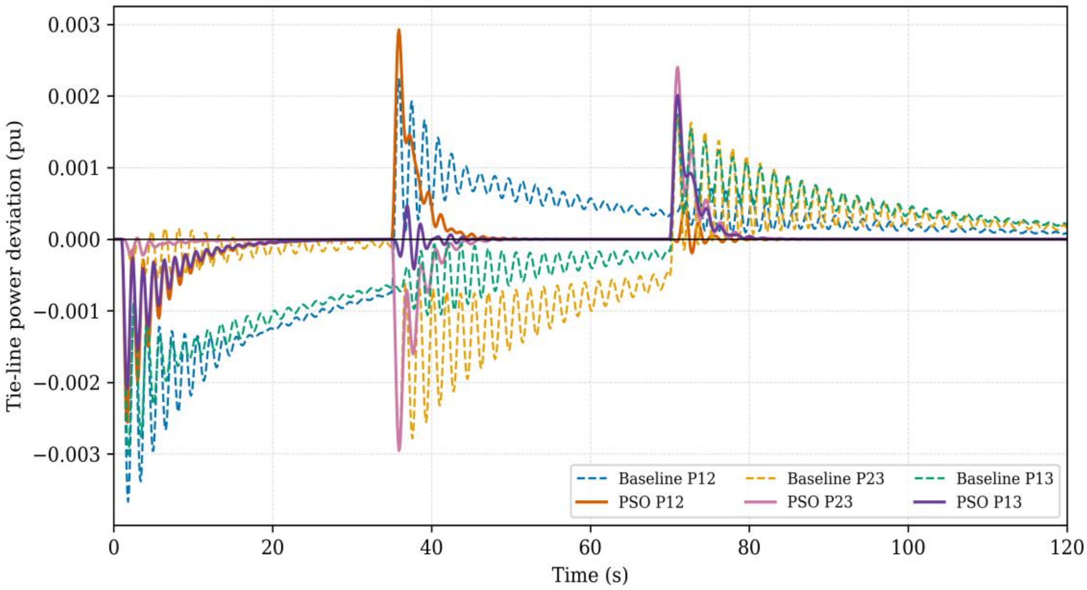

Fig. 5. Three-channel tie-line power deviations for baseline and PSO-optimized control.

The overall maximum tie-line deviation decreases from 0.003666 to 0.002950 p.u., a 19.53% improvement. Channel P12 decreases by 20.22% and P13 by 30.60%, but P23 increases slightly from 0.002914 to 0.002950 p.u. (1.22%). Thus, PSO improves aggregate interchange control without producing a uniform reduction in every bilateral channel. The optimized waveforms nevertheless return close to zero more quickly, indicating improved scheduled-interchange restoration.

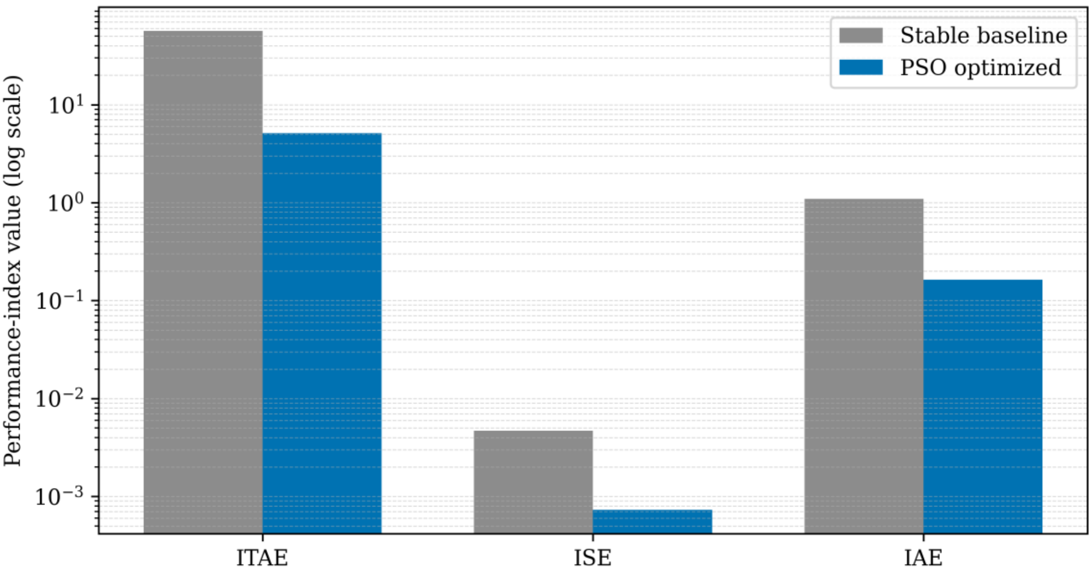

Fig. 6. Integral performance indices for baseline and PSO-optimized control.

The time-domain indices show the strongest overall improvement. IAE decreases from 1.094400 to 0.163389, ISE from 0.004675 to 0.000731, and ITAE from 56.741815 to 5.110215. These changes correspond to reductions of 85.07%, 84.36% and 90.99%, respectively. The especially large ITAE reduction confirms that PSO suppresses persistent late-time error rather than only reducing the initial peak. ITSE is not reported because a verified value was not available in the validated output set.

Table 4. Baseline and PSO-Optimized Dynamic Performance.

Performance measure	Stable baseline	PSO optimized	Change / improvement
Maximum $\|\Delta f\|$ (p.u.)	0.017536	0.014238	18.81% reduction
Area 2 maximum $\|\Delta f\|$ (p.u.)	0.015453	0.013750	11.02% reduction
Area 3 maximum $\|\Delta f\|$ (p.u.)	0.012516	0.010851	13.30% reduction
Maximum $\|\Delta P_{tie}\|$ (p.u.)	0.003666	0.002950	19.53% reduction
Maximum $\|ACE\|$ (p.u.)	0.012191	0.009894	18.85% reduction
Settling time (s)	120.0	77.1	35.75% reduction
Controller energy	0.0131425	0.0185078	40.82% increase

Table 5. Integral Indices and Terminal Restoration.

Metric	Stable baseline	PSO optimized
IAE	1.094400	0.163389
ISE	0.004675	0.000731
ITAE	56.741815	5.110215
Terminal $\Delta f1$ (p.u.)	−0.000995	1.95×10^{-10}
Terminal $\Delta f2$ (p.u.)	−0.001084	-1.28×10^{-10}
Terminal $\Delta f3$ (p.u.)	−0.000784	-9.35×10^{-11}

Tables 4 and 5 jointly show the principal engineering trade-off. PSO yields lower peaks, faster settling and substantially smaller accumulated error, but it requires greater controller energy. The 40.82% energy increase should therefore be considered when selecting actuator limits and generation-rate constraints for practical implementation. Near-zero terminal deviations establish successful secondary frequency restoration, while the remaining channel-specific P23 increase motivates multiobjective weighting or explicit per-line constraints in future studies.

6. CONCLUSION

A standard PSO was applied to nine gains of independent filtered PID controllers in a heterogeneous three-area interconnected LFC system. Under sequential 0.010, 0.008 and 0.006 p.u. disturbances, the optimized design reduced the overall frequency peak by 18.81%, maximum tie-line deviation by 19.53%, maximum ACE by 18.85% and settling time by

35.75%. IAE, ISE and ITAE decreased by 85.07%, 84.36% and 90.99%, respectively, and all three terminal frequency deviations approached numerical zero. These outcomes confirm improved damping, scheduled interchange recovery and secondary frequency restoration. The analysis also identifies two limits: controller energy increased by 40.82%, and P23 peak deviation increased by 1.22% even though aggregate tie-line performance improved. Consequently, the proposed PSO–PID design is best interpreted as a reproducible high-performance benchmark rather than proof of a globally optimal or uniformly superior response across every channel.

7. Future Scope

Future work should incorporate generation-rate constraints, governor dead band, saturation, communication delay and uncertain renewable injections into the same three-area benchmark. Explicit multiobjective PSO can penalize individual tie-line peaks and controller energy instead of relying primarily on an aggregate cost. Battery energy storage, demand response and electric-vehicle participation may be evaluated for faster reserve delivery. Adaptive or hybrid PSO variants should be compared under identical bounds and disturbance sets, followed by Monte Carlo robustness analysis. Real-time digital simulation and hardware-in-the-loop validation are necessary before utility-scale AGC deployment.

REFERENCES

1. M. Wadi et al., “Load frequency control in modern interconnected power systems: A comprehensive review,” Renewable and Sustainable Energy Reviews, vol. 189, Art. no. 114013, 2024, doi: 10.1016/j.rser.2023.114013.
2. A. Latif et al., “Load frequency control of renewable energy based hybrid power systems: A review,” Energy Reports, vol. 7, pp. 4009–4021, 2021, doi: 10.1016/j.egyr.2021.06.088.
3. N. K. Gupta, B. Kar, and A. K. Singh, “Improved sine cosine algorithm-based 2DOF-PID controller for load frequency control of a three-area nonlinear power system,” Protection and Control of Modern Power Systems, vol. 7, Art. no. 33, 2022, doi: 10.1186/s41601-022-00255-w.
4. S. Pahadasingh et al., “Load frequency control of multi-area power systems using JAYA optimization,” Engineering, Technology & Applied Science Research, vol. 12, no. 3, pp. 8646–8651, 2022, doi: 10.48084/etasr.4891.

5. D. V. Doan et al., “Load-frequency control of three-area interconnected power systems using differential evolution,” Engineering, Technology & Applied Science Research, vol. 12, no. 4, 2022, doi: 10.48084/etasr.4924.
6. B. Dhanasekaran et al., “Load frequency control of a standalone multi-source power system using PSO-PID,” Technologies, vol. 11, no. 1, Art. no. 22, 2023, doi: 10.3390/technologies11010022.
7. V. N. Ogar et al., “Particle-swarm-optimized PID control for load-frequency regulation with renewable generation,” Energies, vol. 16, no. 15, Art. no. 5748, 2023, doi: 10.3390/en16155748.
8. R. El-Sehiemy et al., “Fractional-order load-frequency control using chaotic particle swarm optimization,” Fractal and Fractional, vol. 7, no. 1, Art. no. 97, 2023, doi: 10.3390/fractalfract7010097.
9. M. M. Gulzar et al., “Improved swarm-optimized fractional-order control for interconnected load-frequency regulation,” International Journal of Energy Research, Art. no. 5999997, 2023, doi: 10.1155/2023/5999997.
10. W. Younis et al., “Hybrid particle swarm–artificial hummingbird algorithm tuned PID controller for interconnected load-frequency control,” Energies, vol. 17, no. 16, Art. no. 3962, 2024, doi: 10.3390/en17163962.
11. Y. O. M. Sekyere, E. K. Effah, and P. Y. Okyere, “Optimally tuned cascaded FOPI–FOPIDN controller using improved PSO for renewable-integrated interconnected power systems,” Journal of Electrical Systems and Information Technology, vol. 11, Art. no. 25, 2024, doi: 10.1186/s43067-024-00149-x.
12. Z. Qu et al., “Optimized secondary frequency control for renewable-integrated multi-area power systems,” Energies, vol. 17, Art. no. 517, 2024, doi: 10.3390/en17020517.
13. D. N. Chi et al., “Optimized intelligent controllers for frequency regulation in multi-area interconnected power systems,” Applied Sciences, vol. 15, no. 6, Art. no. 2898, 2025, doi: 10.3390/app15062898.
14. M. Z. Yameen et al., “Hybrid intelligent optimization for load-frequency control of interconnected power systems,” Scientific Reports, vol. 15, Art. no. 17549, 2025, doi: 10.1038/s41598-025-01481-6.
15. G. El-Saady et al., “Intelligent optimized control of multi-area load-frequency dynamics,” Virtual Reality & Intelligent Hardware, vol. 7, no. 3, pp. 299–316, 2025, doi: 10.1016/j.vrih.2025.03.006.

16. Y. Chen et al., "Robust nonlinear load-frequency control for interconnected power systems," International Journal of Robust and Nonlinear Control, vol. 35, pp. 3358–3369, 2025, doi: 10.1002/rnc.7847.
17. G. Mustafa, "Fixed-time resilient load-frequency control of interconnected power systems," International Journal of Robust and Nonlinear Control, vol. 35, pp. 1792–1808, 2025, doi: 10.1002/rnc.7756.
18. A. Sharma and N. Singh, "Adaptive load-frequency control for uncertain interconnected power systems," Transactions of the Institute of Measurement and Control, vol. 48, no. 8, 2026, doi: 10.1177/01423312241309066.
19. P. Satapathy et al., "Optimized frequency control of renewable-rich multi-area power systems," Scientific Reports, vol. 16, Art. no. 18630, 2026, doi: 10.1038/s41598-026-49421-2.
20. S. Almutairi et al., "Comparative assessment of PSO-tuned hybrid fuzzy controllers for load-frequency control of a two-area hybrid power system," Energies, vol. 19, no. 11, Art. no. 2677, 2026, doi: 10.3390/en19112677.